A Wide Frequency Range Computation Code for Overhead and Buried Conductor System

R. Andolfato, L. Bernardi, L. Fellin
Department of Electrical Engineering
University of Padova - Italy

Abstract: In this paper a novel computer code for the analysis of both aerial and buried system of conductors in wide frequency range is presented.An hybrid approach has been applied enabling to incorporate into a single linear system both lumped circuit parameters and distributed parameters evaluated through a rigorous electromagnetic field analysis. The system of discretised conductors is replaced by a suitable set of elementary current sources. These current sources may be plain or hollow, bare or insulated, freely oriented and interconnected in the three dimensional space, which is considered formed by two half-spaces each one homogeneous, linear and isotropic. Therefore the code does not pose geometric and topological limitations and enables to compute voltages and currents at the source (boundary) elements as well as vector potentials and electric and magnetic fields anywhere in the surrounding medium.Propagation phenomena and reaction currents in the dispersing medium are duly accounted for; for practical applications, the code may be applied for frequencies up to 1 MHz, thus covering the frequency range of usual interest in power systems. Examples of application are given, namely computation of ground current distribution of a long transmission line under fault conditions and electromagnetic interactions between power systems and transmission systems or other buried passive conductors.

Keywords: Electromagnetic Field, Computer modelling, Electromagnetic interferences, Grounding systems, Distribution system, Residential wiring, Ssafety, Conductive coupling, Inductive coupling, Capacitive coupling.

I. INTRODUCTION

An integral method to solve linear problems in open regions is used in this work. This method, as compared with differential ones, reduces both the number of unknowns and the computation efforts ; the discretization of source surfaces is necessary only in the pre-processing phase and the field analysis can be extended in the whole space. On the contrary, the use of integral methods needs greater efforts to obtain anlytical expressions suitable for the computation of electromagnetic quantities by means of integrals extended to the elementary source surface. To consider the difference of electrical characteristics between air and soil, the images method has been used and the shifting complex images method has been introduced. The follow terminology has been used to simplify the text:

- type A medium indicates an infinity, homogeneus, isotropic and linear medium;
- type B medium indicates an infinity medium composed by two homogeneus isotropic and linear half spaces separated from a plane Σ.

II. MATHEMATIC MODEL

In type A medium the vector and scalar potential generated by conductor networks, approximable with equivalent cylindrical 'thin' conductor segments, in harmonic state are given by the following equations:

$$\dot{\mathbf{A}} = \frac{\mu}{4\pi}\int_L \dot{I}\frac{e^{-\dot{\gamma}r}}{r}d\mathbf{l} \quad (1a) \qquad \dot{V} = \frac{1}{4\pi\dot{\varepsilon}}\int_L \dot{q}\frac{e^{-\dot{\gamma}r}}{r}dl \quad (1b)$$

where $\dot{q}$ and $\dot{I}$ are charge density and longitudinal current along conductor respectively, $\dot{\gamma} = \sqrt{j\omega\mu\dot{\sigma}}$ represents the propagation constant of the medium, $\dot{\sigma} = \sigma + j\omega\varepsilon$ and $\dot{\varepsilon} = \varepsilon + \sigma/j\omega$ indicate the complex conducibility and complex permittivity respectively and l is the coordinate along the conductor axis. The relation between charge and current distributions is $\dot{q} = j\dot{s}/\omega$, where $\dot{s} = d\dot{I}/dl$. Electric and magnetic fields can be calculated as:

$$\dot{\mathbf{E}} = -grad\dot{V} - j\omega\dot{\mathbf{A}} \quad (2a) \qquad \dot{\mathbf{H}} = \frac{1}{\mu}rot\dot{\mathbf{A}} \quad (2b)$$

where vector and scalar potentials are given by (1).
The current distribution along the conductors of the system is given by the following expression:

$$\dot{z}\dot{I} + \frac{\partial\dot{V}}{\partial l} + j\omega\dot{A} = \dot{0} \quad (3)$$

where $\dot{z}$ is the internal impedance for unit length, $\dot{A}$ and $\dot{V}$ are the axial component of the vector potential and the scalar potential on surface of the conductor respectively. Generally (3) can be solved only analytically. Subdividing the conductor system into n segments (elementary sources), with length L_k small with respect to the dimension of conductor network and using (3) relatively at segment k, it follows:

$$\dot{z}_k\dot{I}_k + \sum_{i=1}^{n}\frac{\partial\dot{V}_{ik}}{\partial l} + j\omega\sum_{i=1}^{n}\dot{A}_{ik} = \dot{0} \quad (4)$$

where $\dot{I}_k$ is the longitudinal current. If longitudinal and transversal (leakage) current on both right and left half segments can be assumed to be uniform and equal to their average value then $\bar{\dot{I}}_{kl} = \dot{I}_{kl} - \dot{S}_k/4$ for $0 \le l < L_k/2$ and $\bar{\dot{I}}_{kr} = \dot{I}_{kr} + \dot{S}_k/4$ for $L_k/2 < l \le L_k$ where $\dot{S}_k$, $\dot{I}_l$, $\dot{I}_r$ are the total leakage current and left and right-endpoint current of the segment respectively.
With such assumptions, the integration of the (4) along L_k for left and right half segments holds respectively:

$$\dot{z}_k\frac{L_k}{2}\bar{\dot{I}}_{kl} + \sum_{i=1}^{n}\left[\dot{V}_{ikc} - \dot{V}_{ikl}\right] + \sum_{i=1}^{n}\left[\dot{M}_{ilkl}\bar{\dot{I}}_{il} + \dot{M}_{irkl}\bar{\dot{I}}_{ir}\right] = \dot{0} \quad (5)$$

$$\dot{z}_k\frac{L_k}{2}\bar{\dot{I}}_{kr} + \sum_{i=1}^{n}\left[\dot{V}_{ikr} - \dot{V}_{ikc}\right] + \sum_{i=1}^{n}\left[\dot{M}_{ilkr}\bar{\dot{I}}_{il} + \dot{M}_{irkr}\bar{\dot{I}}_{ir}\right] = \dot{0} \quad (6)$$

where the mutual inductive impedance $\dot{M}_{ij}$ is given by the following equation:

$$\dot{M}_{ij} = j\omega \dot{L}_{ij} = \frac{j\omega}{\dot{I}_i} \int_{L_j} \dot{A}_{ij}\, dl \tag{7}$$

Equations (5) and (6) can be rewritten, in matrix equivalent form, for the whole network conductor as:

$$\begin{bmatrix} [\dot{Z}_{ll}] & [\dot{Z}_{lr}] \\ [\dot{Z}_{rl}] & [\dot{Z}_{rr}] \end{bmatrix} \begin{bmatrix} \{\dot{I}_l\} \\ \{\dot{I}_r\} \end{bmatrix} = \begin{bmatrix} [\dot{Z}_{lt}]\{\dot{I}_t\} \\ [\dot{Z}_{rt}]\{\dot{I}_t\} \end{bmatrix} \tag{8}$$

where *It* represents the injected current in the mid point of the segment. Furthermore, the first Kirchhof's law applied for all segments holds:

$$\{\dot{S}\} = \{\dot{I}_l\} - \{\dot{I}_r\} + \{\dot{I}_t\} \tag{9}$$

Coefficients of (8) are linear combination of internal impedance, mutual inductive impedance and mutual capacitive and conductive impedance (see section 3).

Equation (8) contains all the information about geometric and physical characteristics of the field sources and of the propagation medium. The solution of (8) gives endpoint currents of each elementary segment and using (9) the leakage current can be easily computed. From the longitudinal and transversal current, electric and magnetic fields can be obtained, at any point in the medium, applying the superposition of the effects of the single elementary source.

The number of unknowns of (8) can be reduced by introducing topologic relationships of the conductor network.

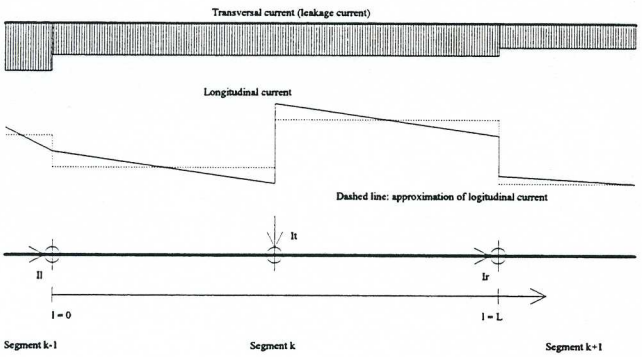

Fig. 1. Approximate distribution of currents in an elementary source.

III. PARAMETERS OF THE MODEL

Coefficients of (8) can be obtained from expression of: the internal impedance of a segment for unit length, the mutual capacitive-conductive coupling coefficient between source and a generic point and the mutual inductive coupling coefficient between two sources. Internal impedance of a metallic cylindrical tube can be computed by using the following equation:

$$\dot{z}_i = \frac{j\omega\mu_c}{2\pi r_0 \dot{\gamma}_c} \frac{I_0(\dot{\gamma}_c r_0) K_1(\dot{\gamma}_c r_0') + K_0(\dot{\gamma}_c r_0) I_1(\dot{\gamma}_c r_0')}{I_1(\dot{\gamma}_c r_0) K_1(\dot{\gamma}_c r_0') - I_1(\dot{\gamma}_c r_0') K_1(\dot{\gamma}_c r_0)} \tag{10}$$

where r_0 and r_0' are the outer and inner radius respectively, $\dot{\gamma}_c$ is the propagation coefficient, I_n and k_n are the modified Bessel functions of order *n* of the first and second kind respectively. The coefficient of the mutual capacitive-conductive coupling between source and a generic point (*p*) represents the ratio between the scalar potential generated from the source in (*p*) and the leakage current from the whole source. Now, let $\dot{\rho} = 1/\dot{\sigma}$ be the complex resistivity. If the coordinate system shown in Fig. 2 is assumed, the application of (1b) in the case of a conductor segment which leaks current uniformly in the surrounding medium and in the case of point-source, both located in a type A medium, leads to the following equations:

$$\dot{V} = \dot{\rho}\dot{S}\Psi \qquad \text{(11a)} \qquad\qquad \dot{V} = \dot{\rho}\dot{S}\psi \qquad \text{(11b)}$$

where:

$$\Psi = \frac{1}{4\pi L} \int_L \frac{e^{-j\dot{\gamma}r}}{r} dl \qquad \text{(12a)} \qquad\qquad \psi = \frac{1}{4\pi} \frac{e^{-j\dot{\gamma}r}}{r} \qquad \text{(12b)}$$

Equations (11a) and (11b) allow to obtain the scalar potential associated to both the leakage current $\dot{S}$ from the elementary source along its total lenght and the currents $\dot{I}_l$ e $\dot{I}_r$ flowing at the source endpoint (see also Fig. 1). Suppose a type B medium and assume the following symbology: *n* indicates the half-space in which the source is located, *j* indicates the opposite half-space, *m* indicates the half-space containing the observation point and *i* indicates the opposite half-space. Now let $\upsilon = (\dot{\rho}_j - \dot{\rho}_n)/(\dot{\rho}_j + \dot{\rho}_n)$ and δ_{mn} be the reflection coefficient corresponding to medium *n* and medium *j* and the Kronecker's delta respectively.

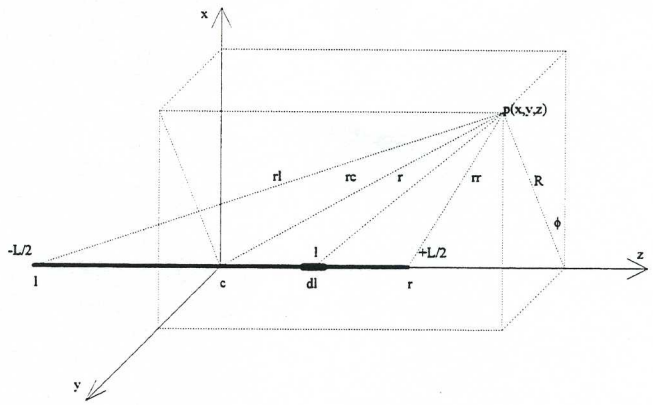

Fig. 2. Coordinate system

Expressions of the mutual capacitive-conductive coupling coefficient both between conductor segment and a generic point and between a point-source and a generic point can be obtained using the Images Method (IM) and equations (11a) and (11b). Such expressions assume the following forms respectively:

$$\dot{K} = \dot{\rho}_m \left[(1 - \upsilon + \upsilon\delta_{mn})\Psi + \upsilon\delta_{mn}\Psi' \right] \tag{13a}$$

$$\dot{k} = \dot{\rho}_m \left[(1 - \upsilon + \upsilon\delta_{mn})\psi + \upsilon\delta_{mn}\psi' \right] \tag{13b}$$

where the quantities marked with apex indicate contributions of images sources. Coefficient $\dot{k}$ holds in (8) the information about the topology of the conductor network.

The mutual inductive coupling coefficient between two generic sources is defined by (7). Consider the coordinate system shown in Fig.2 and suppose a type A medium: if the longitudinal current is assumed to be constant along the length of the elementary source, then (1a) can be rewritten as:

$$\dot{\mathbf{A}} = \mu \dot{I} L \Psi \frac{\mathbf{z}}{z} \tag{14}$$

where Ψ is given by (12a). Now consider the particular coordinate system shown in Fig.3 (in which the source is situated on plane *Y=0* without any loss of generality) and suppose a type B medium. In this

case, using the symbology introduced above and indicating with 1 and 2 soil layer and air layer respectively, horizontal and vertical components of the vector potential generated by an elementary segment can be written as follows:

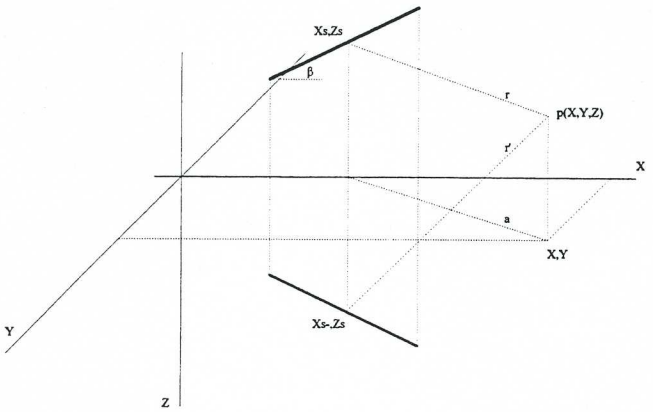

Fig. 3. Coordinate system

$$\dot{A}_X = \frac{\mu_m \cos\alpha_X}{4\pi}\int_L \left[(g_m - g_m')\delta_{mn} + U\right]\dot{I}dl \tag{15}$$

$$\dot{A}_Z = \frac{\mu_m}{4\pi}\int_L \left\{\operatorname{sen}\beta\left[(g_m - g_m')\delta_{mn} + V + \cos\beta\frac{\partial W}{\partial X}\right]\right\}\dot{I}dl \tag{16}$$

where $g_m = e^{-\dot{\gamma}_m r}/r$ represents Green's function for the medium m and U, V, W represent Sommerfeld's integrals. At low frequencies and accounting for electrical characteristics of soil and air, the above integral expressions can be approximated as follows:

$$U \cong \sum_{i=1}^{k} \dot{a}_i \frac{e^{-\dot{\gamma}_e \dot{r}_i}}{\dot{r}_i} \tag{17}$$

$$V \cong 0 \quad \text{(if n=1)} \qquad (18a), \qquad V \cong 2\sum_{i=1}^{k} \dot{a}_i \frac{e^{-\dot{\gamma}_e \dot{r}_i}}{\dot{r}_i} \quad \text{(if n=2)} \qquad (18b)$$

$$W \cong -\sum_{i=1}^{k} \dot{a}_i I_0\left[\frac{\dot{\gamma}_e}{2}(\dot{r}_i - \dot{b}_i)\right] K_0\left[\frac{\dot{\gamma}_e}{2}(\dot{r}_i + \dot{b}_i)\right] \tag{19}$$

where:

- $\dot{r}_i = \sqrt{a^2 + \dot{b}_i^2}$
- $a^2 = (X - X_s)^2 + (Y - Y_s)^2$
- $\dot{\gamma}_e = \dfrac{\dot{\gamma}_n\left(|Z|\delta_{mn} + |Z_s|\right) + \dot{\gamma}_m\left(|Z| + |Z_s|\delta_{mn}\right)}{\left(|Z_s| + |Z|\right)(1 + \delta_{mn})}$

and k depends on the degree of approximation required.

From (15) and (16) together with expressions (17) to (19), the components of the vector potential due to a source parallel to Σ can be rewritten as:

$$\dot{A}_X^X = \mu_0 \dot{I} L^X \left[(\Psi - \Psi')\delta_{mn} + \sum_{i=1}^{k} \dot{a}_i \Psi_i\right] \tag{20}$$

$$\dot{A}_Z^X = \mu_0 \dot{I} L^X \sum_{i=1}^{k} \dot{a}_i \Xi_i \tag{21}$$

where:

- $$\Xi_i = \frac{1}{4\pi L^X}\left\{I_0\left[\frac{\dot{\gamma}_e}{2}(\dot{r}_{li} - \dot{b}_i)\right] K_0\left[\frac{\dot{\gamma}_e}{2}(\dot{r}_{li} + \dot{b}_i)\right] - I_0\left[\frac{\dot{\gamma}_e}{2}(\dot{r}_{ri} - \dot{b}_i)\right] K_0\left[\frac{\dot{\gamma}_e}{2}(\dot{r}_{ri} + \dot{b}_i)\right]\right\}$$

while for a source perpendicular to Σ:

$$\dot{A}_X^Z = \dot{0} \tag{22}$$

$$\dot{A}_Z^Z = \mu_0 \dot{I} L^Z (\Psi - \Psi')\delta_{mn} \quad \text{(if n=1),} \tag{23a}$$

$$\dot{A}_Z^Z = \mu_0 \dot{I} L^Z \left[(\Psi - \Psi')\delta_{mn} + 2\sum_{i=1}^{k} \dot{a}_i \Psi_i\right] \quad \text{(if n=2)} \tag{23b}$$

Equations (20)÷(23b) provide contribution of real sources and images sources to the vector potential. The subscript i in the summation indicates the order of images: longitudinal current and location of these images are defined from complex coefficients $\dot{a}_i$ e $\dot{b}_i$ respectively. Greater is the order of image lower is its contribution either because the distance between images and observation point increase or because the longitudinal current of the images reduces. Their location is defined in a coordinate system which has two real axis situated on plane Σ and a third complex axis perpendicular to the same plane. If the observation point changes, images shift along the complex axis hence it follows the name Shifting Complex Images Method (SCIM) assigned to this computing method. From expression of vector potential, the mutual inductive coupling coefficient can be computed through numerical integration of (7).

IV. ELECTRIC AND MAGNETIC FIELD

From the longitudinal and leakage currents of each elementary source together with IM and SCIM, it is possible to calculate the electric and magnetic field at any point in the surrounding medium as vectorial superposition of effects due to the elementary sources. In a type B medium, the electric field is generally expressed by (2a) where the scalar and vector potential are given by expressions written above:

$$\dot{\mathbf{E}} = -grad\sum_{i=1}^{n} \dot{\rho}_m \dot{S}_i\left[(1 - \dot{\upsilon} + \dot{\upsilon}\delta_{mni})\Psi_i + \dot{\upsilon}\delta_{mni}\Psi_i'\right] - j\omega\sum_{i=1}^{n}\left(\dot{\mathbf{A}}_{Xi}^X + \dot{\mathbf{A}}_{Zi}^X + \dot{\mathbf{A}}_{Xi}^Z + \dot{\mathbf{A}}_{Zi}^Z\right) \tag{24}$$

Magnetic field is given by (2b). Algebrical manipulation of (2b) together with expressions (20)÷(23b) lead to the following equation:

$$\dot{\mathbf{H}} = \frac{1}{\mu}\operatorname{rot}\sum_{i=1}^{n}\left(\dot{\mathbf{A}}_{Xi}^X + \dot{\mathbf{A}}_{Zi}^X + \dot{\mathbf{A}}_{Xi}^Z + \dot{\mathbf{A}}_{Zi}^Z\right) \tag{25}$$

Equations (24) and (25) take into account contributions of both real sources and images sources defined from IM and SCIM.

V. RANGE OF APPLICATION OF THE COMPUTING CODE

The methodology illustrated above has been implemented in the computer program AGSA (Aerial and Grounding System Analysis). Limit of AGSA application are due both to initial hypotesis and to symplifications assumed for computing the Sommerfeld's integrals. Most important limits are: $f_1 \le 10^6$ because Sommerfeld's integral have not been considered in the calculation of electrostatic field; $f_2 \le 1/20\pi\rho_1\varepsilon_0$ in order the modulus of soil complex conducibility to be much greater than that of the air; finally $f_3(k) \le \left(g_k^2\rho_1\right)/\left(2\pi\mu_0\right)$ (where g_k depends on the number k of the complex images taken into account) in order to hold the propagation constant of the soil small enough. The range of application of AGSA can be graphically represented as shown in Fig. 4.

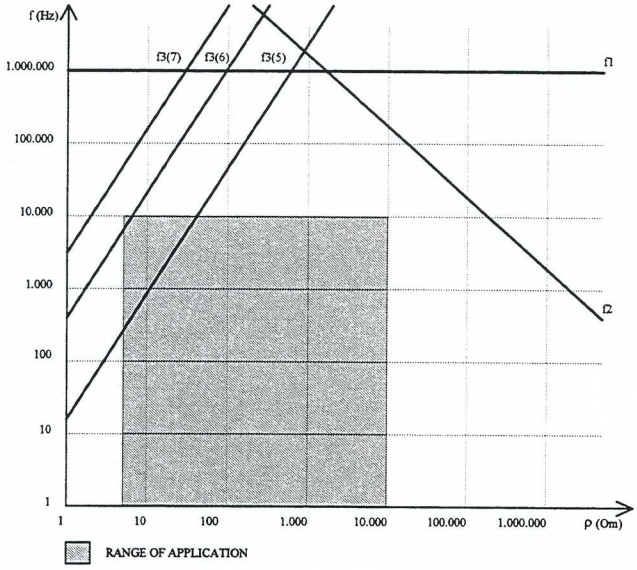

Fig. 4. Range of application of computing code

It covers the whole employment field of usual application in electric power systems. The frequency range of application includes sub-synchronous, synchronous, harmonic and free evolution state. In terms of resistivity, the field of application ranges from values typical of sea water to values pertinent to rocky and dry soil and higher.

VI. APPLICATIONS

Description of typical applications of AGSA.

A. Zero-sequence current returning trought soil

In a circuit closed to soil, path configuration of an alternate current in the ground is due to inductive coupling with the section of the circuit insulated from earth. If the current is direct, the mentioned coupling does not exist and the current flows trought the minimum resistance path. Fig. 5 shows the physical situation considered in this example: a zero-sequence current *I* flows along a part of an aerial line between feeding-station and a point in which a single-phase to ground fault is occurred. The circuit is closed to soil throught ground fault and earth grid of the station. It is assumed an uniform earth (ρ =100 Ωm) and *I*=500 A. The analysis is carried on at two frequencies: f=0 Hz and f=50 Hz. Distributions of the currents density calculated in the ground over the horizontal surface A shown in Fig. 5 are displayed in Fig. 6 and 7 respectively. In the first case, the density presents only two peaks corresponding to the two connecting-points to soil of the aerial line; in the second one, Fig. 7 shows clearly that the current, because of the inductive coupling, flows in the earth in the zone below the aerial line. This phenomenon is confirmed observing Fig. 8 which graphs the magnitude of current density computed on the vertical surface B shown in Fig. 5

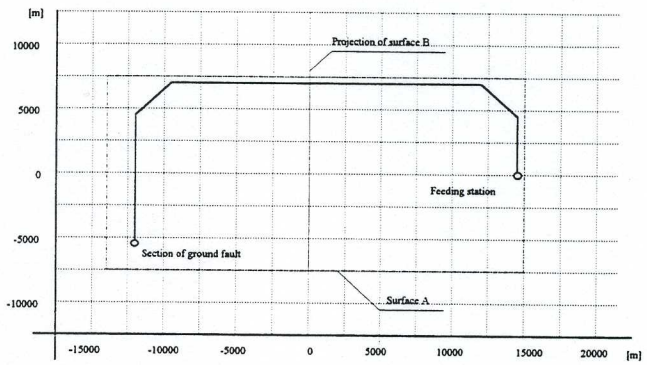

Fig. 5. Physical situation

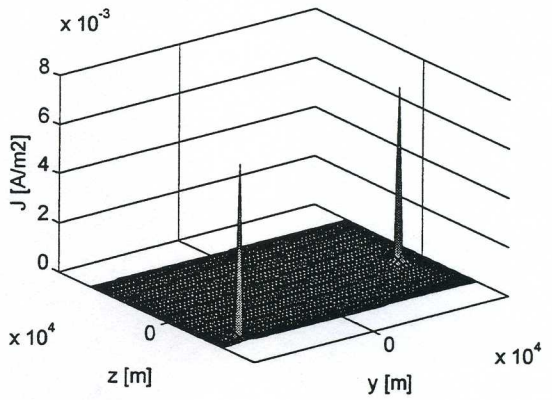

Fig. 6. Distribution of current density calculated on surface A (f = 0 Hz)

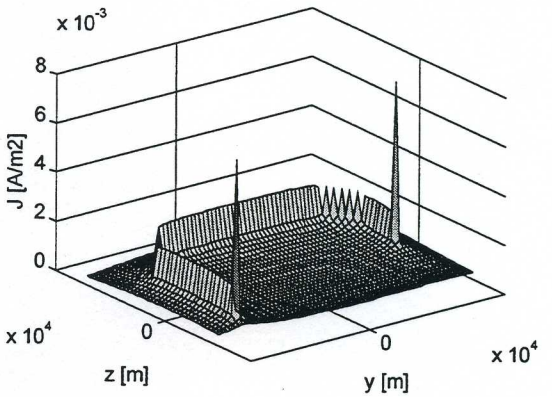

Fig.7. Distribution of current density calculated on surface A (f =50 Hz)

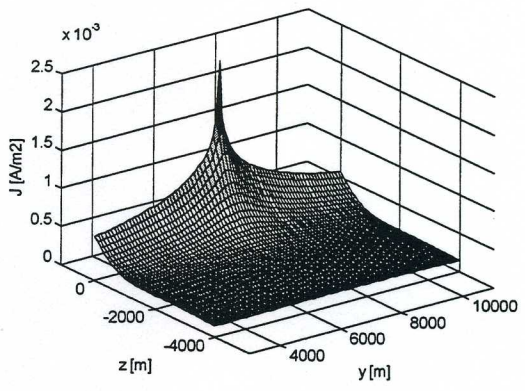

Fig.8. Distribution of current density calculated on surface B (f =50 Hz)

B. Interference between electric power systems and communication systems

Communication lines can be coupled in inductive, capacitive or conductive way with power-transmission lines. Because of such couplings, disturbing voltages can appear on the communications lines. AGSA allows to analyse this problem considering, at the same time, all three forms of couplings. Normally, in practical cases, the effect of the inductive coupling is predominant over the others. Fig. 9 shows the physical situation considered in this example: a 4,5 kA ground fault current flows along a power-transmission line at 50 Hz.

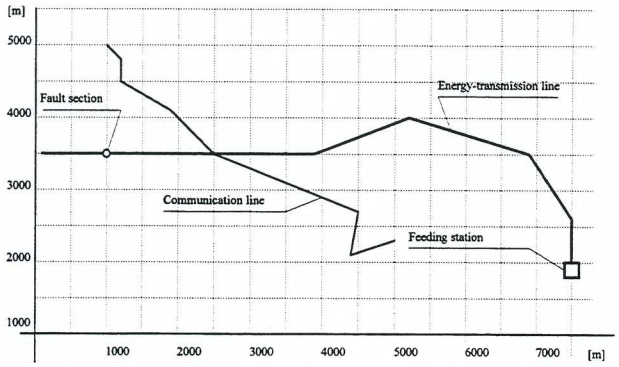

Fig. 9. Physical situation

As can be seen in Fig. 10 shows, for all fault duration, the induced voltage on the communication line can reach values such to create dangerous situations for the line itself.

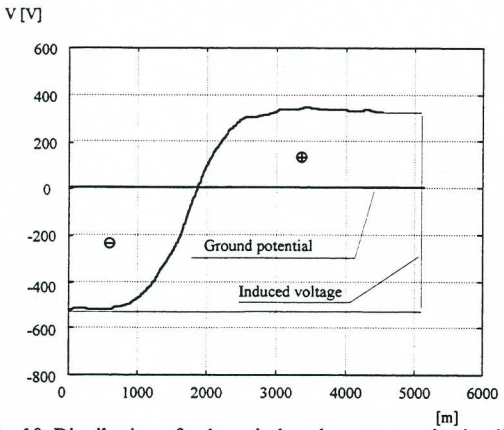

Fig. 10. Distribution of voltage induced on communication line (f=50 Hz)

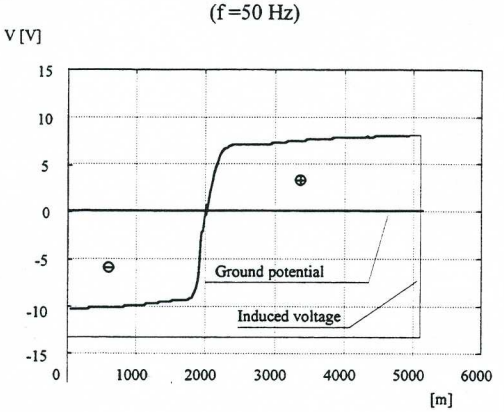

Fig. 11. Distribution of voltage induced on communication line (f=10 kHz)

If a 4,5 A current at 10 kHz flows along the transmission line, the induced voltage is clearly lower (see Fig. 11) but remaining constant in the time can generate noises to the communications. In the first case (f=50 Hz), results of AGSA are successfully compared to results provided by CCITT for the same physical situation.

C. Interaction between high-voltage lines and buildings

The distribution of electric and magnetic field generated from high-voltage lines, are influenced by the presence of buildings located in their vicinity. This phenomenon can be analysed by means of AGSA. Consider the physical situation of Fig. 12: a 500 A current flows along an energy-transmission line (rated voltage 220 kV) which has a building 25 m heigth in its proximity, schematically represented by its principal reinforcements.

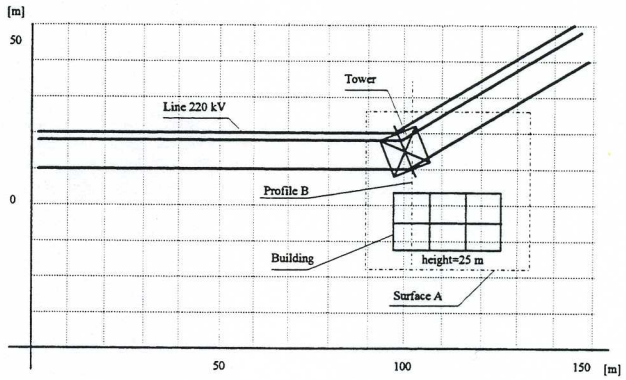

Fig. 12. Physical situation

Figures 13 and 14 graph the distribution of electric and magnetic field, computed at 11 m over the soil on surface A of Fig 12. The electric field increases in the zone situated between building and line while it is reduced elsewhere. The effect of the construction is due to the transfer of ground potential through reinforcements connected to the earth. The influence of the building on the distribution of the magnetic field is hardly perceptible and obviously subsists only if reinforcement form a closed circuit. Figures 15 and 16 show the distribution of electric and magnetic field computed at 5 m over the soil surface along profile B of Fig. 12. They are useful to have quantitative information about the phenomenon discussed above.

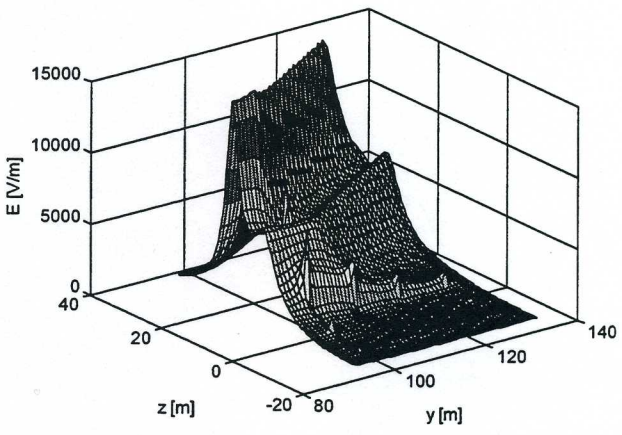

Fig. 13. Distribution of electric field calculated at 11 m over the earth surface

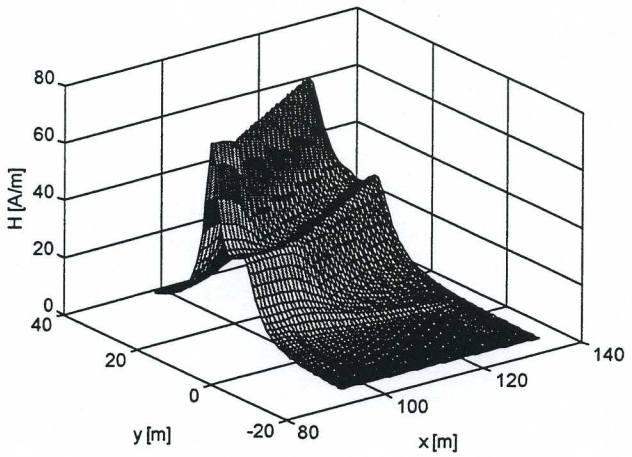

Fig. 14. Distribution of magnetic field calculated at 11 m over the earth surface

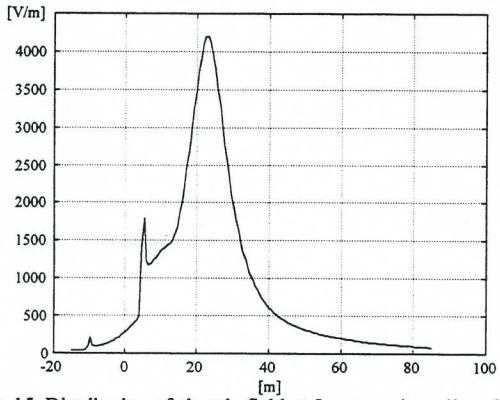

Fig. 15. Distribution of electric field at 5 m over the soil surface.

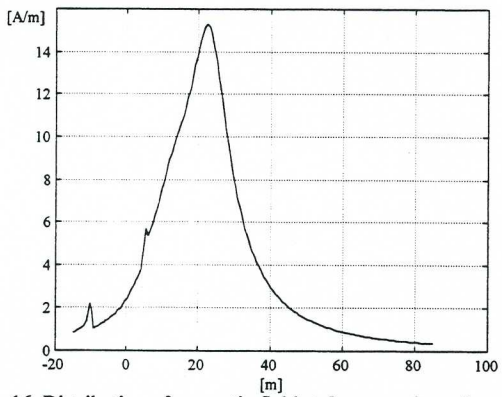

Fig. 16. Distribution of magnetic field at 5 m over the soil surface

D. Interaction between ground grid and other buried electrodes

The current injected in the soil from ground grid can affect other metallic structures (pipeline, railroads etc...) buried in its vicinity. This interference may cause hazards and possibly severe stresses on these structures. The compatibility between different systems can be analysed through AGSA. Fig. 17 shows the physical situation considered in this example: a ground grid injects in the soil a 100 A fault current at 50 Hz. It has, in its proximity, a tug of oil pipeline delimited by insulating joints indicated with letters A and B in Fig.17. The pipeline, made of steel ($\rho=10^{-7}$ Ωm), has a 400 mm diameter.The soil is assumed to be uniform with resistivity 100 Ωm.

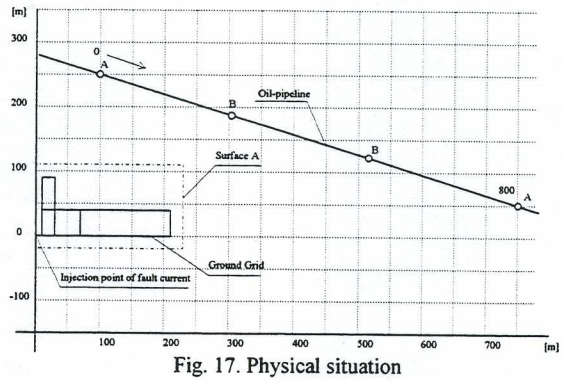

Fig. 17. Physical situation

Fig. 18 shows the longitudinal current along the oil pipeline both in the presence of only insulating joints A and adding joints B: in the second case the maximum value of current transferred from pipeline is lower than that obtained in the first case.

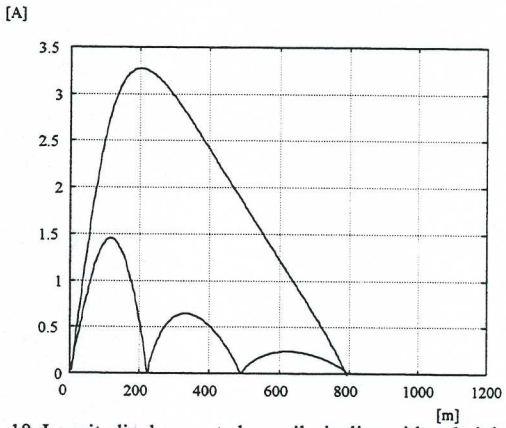

Fig. 18. Longitudinal current along oil-pipeline with only joints A and adding joints B.

The slope of the curves shown in Fig. 18 gives information about the earth leakage current density along the pipeline. If the ground network belongs to the electric-traction plant (normally operated in direct current), the example considered in this section can be used to analyse corrosive effects due to eddy currents. Figures 19 and 20 graph the distribution of electric and magnetic field calculated on earth surface respectively: while the distribution of electric field depends on the distribution of the leakage current from the grid and presents peak values at the corner of the ground network where leakage is greater, magnetic field is closely in relation with longitudinal current along conductor network and presents greater values near the injection point of the fault current

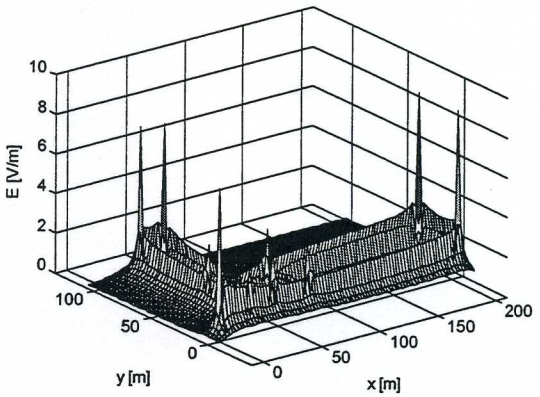

Fig. 19. Distribution of electric field computed on surface A.

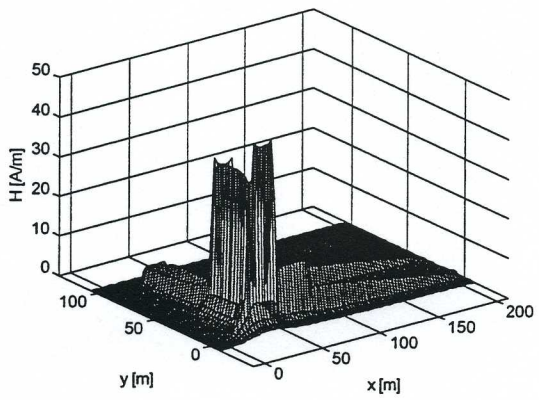

Fig. 20. Distribution of magnetic field computed on surface A.

VII. CONCLUSIONS

A computing code for the analysis of both aerial and buried system of conductors in wide frequency range has been described. The computer code based on integral methods is advantageous, as compared with differential ones, to solve linear problems in open regions. To study a medium formed by two half-spaces with different characteristics the well-known Images Method (IM) has been used and the Shifting Complex Images Method (SCIM) has been developed. These complex images derive from Sommerfeld's integral. The range of application of the method has been specified : it can be applied up to 1 MHz, thus covering the frequency range of usual interest in power systems. Analytical developments have required considerable efforts. On the other hand this allows to obtain algorithms that reduce computation task. Thus the computer program derived (AGSA) can run on a normal Personal Computer. The generality of the approach assumed in this paper enables on the one hand to have a flexible computing code, on the other hand to incorporate into a single linear system both lumped circuit parameters and distributed parameters evaluated through a rigorous electromagnetic field analysis. Typical applications of interest in power systems in the frequencies range 0÷10 kHz has been briefly decribed.

VIII. REFERENCES

[1] A. Sommerfeld, "Uber die ausbrilung der wellen in draftlosen telegraphe", Annalen der Physik, 4th folge, vol. 28, pp. 665-736, 1909.

[2] L.Grcev, F. Dawalibi, "An electromagnetic model for transients in grounding systems", IEEE Transactions on Power Delivery, vol. 5, n. 4, pp. 1773-1781, novembre 1990.

[3] F. Dawalibi, A. Selby, "Electromagnetic fields of energized conductors", IEEE Transactions on Power Delivery, vol. 8, n. 3, pp. 1275, 1284, luglio 1993.

[4] S.A. Schelkunoff, Electromagnetic Waves, Princeton N.J., D. Van Nostrand Compahy Inc., 1943.

[5] E.D. Sunde, Earth Conduction Effects in Transmission Systems, New York, D. Van Nostrand Compahy Inc., 1949.

[6] R.F. Harrington, Field computation by moment methods , R.E. Krieger publishing company, Florida, 1968.

[7] M. Abramovitz, I.A. Stegun, Handbook of Mathematical Functions, Dover Publications Inc., New York, 1970

[8] CCITT, Directives concerning the protection of telecommunication lines against harmful effects from electric power and electrified railway lines, Vol. II e III, Geneva, 1989.

IX. BIOGRAPHIES

Roberto Andolfato received a dr.ing. degree in electrical engineering from University of Padova in 1990 and is presently concluding his Ph.D. course at the same university. His main field of interest is power system earthing with specific emphasis at developing numerical procedures for simulating the electromagnetic field generated by complex geometries in disperding media. He also is a professional consultant engineer and a member of the Italian Electrical and Electronic Association (AEI).

Luca Bernardi received a dr.ing. degree in electrical engineering from University of Padova in 1997 and is actually attending his Ph.D. course at the same university. His branch of research is electromagnetic interferences between electric power installations and other systems . He is also a member of the Italian Electrical and Electronic Association (AEI).

Lorenzo Fellin received a dr.ing. degree in electrical engineering from University of Padova in 1967 . He joined the Electrical Engineering Dept. of the University of Padova in 1968 where, from 1968, he is Full Professor of Electric Power Installations. He was actively involved in the design and construction of a large laboratory for thermonuclear fusion research (the RFX experiment built-up in Padova with Euratom-ENEA-CNR support). His field of interests also include design of industrial electric installations and electric lighting design. He is a member of IEEE and of the Italian Electrical and Electronic Association (AEI). He also is one the chairmen of the italian association of electric lighting (AIDI).